Journal of Electroanalytical Chemistry 947 (2023) 117759

Contents lists available at ScienceDirect

Journal of Electroanalytical Chemistry

journal homepage: www.elsevier.com/locate/jelechem

Isotope effects in the electrodeposition of Ag and Pd

Kimmo Pyyhtiä, Pekka Peljo *

Department of Mechanical and Materials Engineering, University of Turku, 20500, Finland

ARTICLE INFO

Keywords:
Electrodeposition
Isotope effect
Nucleation mechanism
Kinetic parameters

ABSTRACT

The influence of solvent and its isotope in electrochemical deposition of silver and palladium on pencil graphite from H_2O, D_2O and MeCN was examined via cyclic voltammetry, chronoamperometry and SEM imaging. The evaluation of the nucleation process was done by comparing the current transients to Scharifker–Hills model of nucleation and the process for all samples was deemed to be progressive and mostly under diffusion control. Kinetic parameters were extracted from I/t curves by curve fitting to Heerman–Tarallo model and it was found that for silver and palladium electrodeposition the isotope of the solvent has a noticeable effect on nucleation rate constant with only a limited effect on the number density of nucleation sites.

1. Introduction

In today's world there is ever growing need for new materials and new ways to manufacture them. Nanotechnology is one of the forefronts of materials research as nanoscale structures have vastly different properties than their large-scale counterparts. One of the primary ways of manufacturing structures in nanoscale is electrodeposition, which has been used to produce nanoparticles [1–3], nanodendrites [4,5], nanorods [6,7] and thin films [8–10]. However, electrodeposition on nanoscale is sensitive to many variables and thus it's vital to understand the phenomena governing the electrodeposition processes, such as nucleation, growth, diffusion, and deposition kinetics, to create nanostructures of desired size, shape, and composition. In this study, our focus is on investigating nucleation and kinetics of Ag and Pd. The kinetics and nucleation of an electrodeposition process can be studied from potentiostatic current density-time transients via various theoretical frameworks [11]. The Scharifker–Hills model [12] provides a way to examine the deposition mechanism by rendering the current (I) and time (t) dimensionless by scaling the current data by the peak current I_{max} and peak time t_{max}, and comparing them to two guideline plots. The model assumes diffusion-controlled growth of hemispherical nuclei and is based on three-dimensional multiple nucleation and results in two different mechanisms, instantaneous and progressive nucleation. In instantaneous nucleation, all nuclei form at the very instance of the applied potential step, after which the nuclei grow at the same rate, whereas in progressive nucleation, some nuclei form initially but many are activated progressively, thus resulting in different growth rates for nuclei of varying ages.

The Scharifker–Hills model does however have its limitations, and deviations from it have widely been reported in literature [13–17]. Most often these deviations occur at $t > t_{max}$, and over the years, many models have introduced corrections to explain these deviations [18]. Scharifker et al. [19] suggested that a change in the polarization state of the electrode surface by e.g. hydrogen evolution would cause the apparent additional electrochemical reaction causing the deviation. This correction works well at more negative potentials where hydrogen evolution is present, but has difficulties in explaining electrodeposition of some single-metal salts, which have relatively low polarization [20].

One approach for correcting the deviations was introduced by Heerman and Tarallo [21], where they reported general equations which corrected the conflicting predictions by Scharifker and Mostany [22] and Sluyters-Rehbach et al. [23] by combining elements of both theories and introducing the variable Φ, which is related to Dawson integral, reflecting the deceleration of the current due to sluggish nucleation. Heerman–Tarallo model also offers an easy access to the kinetic parameters straight from the fitting parameters.

The electrodeposition process can be modified to obtain desired morphology, surface area, particle size etc. of the deposit by the use of different potentials, current densities, electrolytes, temperatures and additives [18]. Electrolyte solvent's, specifically, water's, isotope effect has not been widely studied with regards to the nucleation process and the kinetic parameters. The kinetic isotope effects are dependent on the mass differences of the different isotopes, so the largest effects are seen in isotopes of hydrogen, where deuterium has 100% and tritium has 200% more mass than protium. Generally, isotopic effects can be attributed to "primary" effects involving isotopic sub-

* Corresponding author.
E-mail address: pekka.peljo@utu.fi (P. Peljo).

https://doi.org/10.1016/j.jelechem.2023.117759
Received 26 June 2023; Received in revised form 26 August 2023; Accepted 29 August 2023
Available online 4 September 2023
1572-6657/© 2023 The Author(s). Published by Elsevier B.V. This is an open access article under the CC BY license (http://creativecommons.org/licenses/by/4.0/).

Table 1
The different liquid samples used in the experiments and their equilibrium potentials with respect to Ag/AgCl reference electrode. *For $AgNO_3$ in MeCN the crossover potential is taken as E_{eq}.

Active species	c [mM]	Supporting electrolyte	c [mM]	Solvent	E_{eq} [mV]
$AgNO_3$	1	NaCl	3000	H_2O	6
$AgNO_3$	1	NaCl	3000	D_2O	3.3
$AgNO_3$	1	$LiClO_4$	100	MeCN	-27*
$PdCl_2$	1	NaCl	3000	H_2O	24
$PdCl_2$	1	NaCl	3000	D_2O	26

stitution of atoms involved in the reactions, while "secondary" effects involve isotopic substitution close to the atoms involved in the reactions. In electrochemistry, it's been known since the 1960s that isotope effects affect homogeneous electron transfer between transition-metal complexes [24–26]. In electrocatalysis, strong primary effects are observed for reactions involving protons or deuterons [27,28], such as hydrogen [29–33] and oxygen [33–36] evolution. Interestingly, even inverse kinetic isotope effects have been observed for oxygen evolution on Ni and Co [37]. Solvent isotope effects upon the kinetics of some simple outer sphere electron transfer reactions have also been studied for transition-metal complexes of aquo, ammine or ethylenediamine ligands at mercury electrodes [38]. For electron transfer of metal complexes, the isotope effects are attributed to "secondary" isotope effects arising from differences in reactant-solvent and product-solvent interactions and "primary" effects arising from replacement of the H_2O by D_2O in the coordination sphere of the species undergoing charge transfer reactions [38]. Additionally, the electric double layer is affected: for example the measured capacitance of mercury electrode in contact with KF solutions is slightly smaller in D_2O tan in H_2O [39]. Electrochemical techniques have also been developed for intercalation-based or electrodeposition based separation of ^6Li from ^7Li [40–42]. Interestingly, no report on solvent isotope effects on electrodeposition has been reported. Therefore, it is anticipated that studying solvent isotope effects could shed light on interactions of solvent with the dissolved metal and the metal surface.

In this work, the influence of solvent in electrodeposition of silver and palladium on pencil graphite from H_2O, D_2O and MeCN was examined. The evaluation of the nucleation process was done according to the Heerman–Tarallo model, showing that the isotope of the solvent has a noticeable effect on nucleation rate constant but only a limited effect on the number density of nucleation sites.

2. Experimental details

2.1. Chemicals and materials

Electroactive species were deposited on pencil graphite (Pentel Ain Stein, 0.5 mm B) from solutions made in ultrapure water (Milli-Q Direct-Q 5 UV, >18 M Ω· cm), deuterium oxide (Armar isotopes 99.8%) and acetonitrile (J.T. Baker). Electrodeposition of Ag^+ was performed from 1 mM $AgNO_3$ (Sigma-Aldrich, 99.9%) with 3 M NaCl (VWR) or in acetonitrile with 100 mM $LiClO_4$ (Sigma-Aldrich) whereas Pd^{2+} was deposited with solutions of 1 mM $PdCl_2$ (Sigma-Aldrich) and 3 M NaCl (VWR), refer to Table 1. All electrolytes were bubbled with N_2 gas for at least 30 minutes prior to each experiment to remove oxygen from the solution.

2.2. Measurements

All electrochemical measurements were performed in an ambient temperature of approximately 297 K in a borosilicate glass vial with 12 mL of the respective solution with a three-electrode setup using a 3 M KCl Ag/AgCl reference electrodes (+0.210 V vs SHE), and a straight Pt wire with surface area of 0.283 cm^2 in solution as the counter electrode (CE). The pencil graphite rods had the same exposed surface area as the CE and were exchanged with fresh ones after each cyclic voltammetry or chronoamperometric measurement. The graphite rods were not pretreated due their uniform quality resulting from strict quality control during the manufacturing process and because there was no need to pre-activate the electrodes as might be required for very dilute solutions [43]. Potentials in this work are presented with respect to Ag/AgCl RE or overpotential scale although it should be noted that Ag/AgCl RE was not stable in acetonitrile, so its equilibrium potential E_{eq} is taken to be the potential where CV return scan becomes positive, labeled as crossover potential, as shown in Fig. 1c. The equilibrium potentials were measured as the potential difference of Ag or Pd wire placed in the solution and the Ag/AgCl reference electrode filled with aqueous filling solution. The solvent liquid junction potential between H_2O and D_2O solutions is probably negligible (<1-2 mV), as shown earlier [38]. As the formal potential difference between chloride complexes is D_2O and H_2O is on the same order of magnitude, this indicates that Pd^{2+} and Ag^+ are present as chloride complexes with no significant isotopic solvent effect from the complex-solvent interaction. Transformation to overpotential scale is done via Eq. (1) by subtracting the respective equilibrium potential, as presented in Table 1, giving the overpotential,

$$\eta = E - E_{eq}, \tag{1}$$

with E: applied potential, E_{eq}: measured equilibrium potential.

The electrochemical measurements, cyclic voltammetry and chronoamperometry, were carried out with Gamry Instruments Reference 600+ potentiostat. The scan rate for cyclic voltammetry was 50 mV/s.

3. Results and discussion

3.1. Cyclic voltammetry

Electrodeposition of the electroactive species was initially examined with cyclic voltammetry where the polarization curves were measured starting from +0.6 V and scanned between +0.6 V and -0.6 V vs Ag/AgCl reference electrode and are presented in Fig. 1. During the first scan the cathodic peak associated with deposition of the active species was around at -430 mV for Ag in H_2O and D_2O, and -500 mV in MeCN, whereas the cathodic peak for palladium appeared at -324 mV in H_20 and at -300 mV in D_2O vs Ag/AgCl.

On the return scan, anodic peaks where the metal deposits dissolve to the solution are observed at 44 mV, 46 mV and 105 mV for Ag in H_2O, D_2O and MeCN, respectively, and at 490 mV and 405 mV for Pd in H_2O and D_2O, respectively. It is noteworthy that the anodic peak of Fig. 1e Pd in D_2O appears to split in two overlapping peaks which has been explained by there being two phases of dissolving metal, i.e. metal hydride and corresponding pure metal phase [44]. It has also been observed, that repeated scans show the first anodic peak, related to dissolution of palladium hydride, dominates over the second peak associated with dissolution of metallic palladium [45]. As to why in our measurements this anodic peak splitting is seen only in with D_2O, the slight differences in Pd Pourbaix diagrams or the stability constants of the complexes could offer an explanation, but these have not been reported in literature for D_2O.

On subsequent scans, all of the metal deposits that were not stripped off during the anodic scans act as new nucleation sites for deposition of

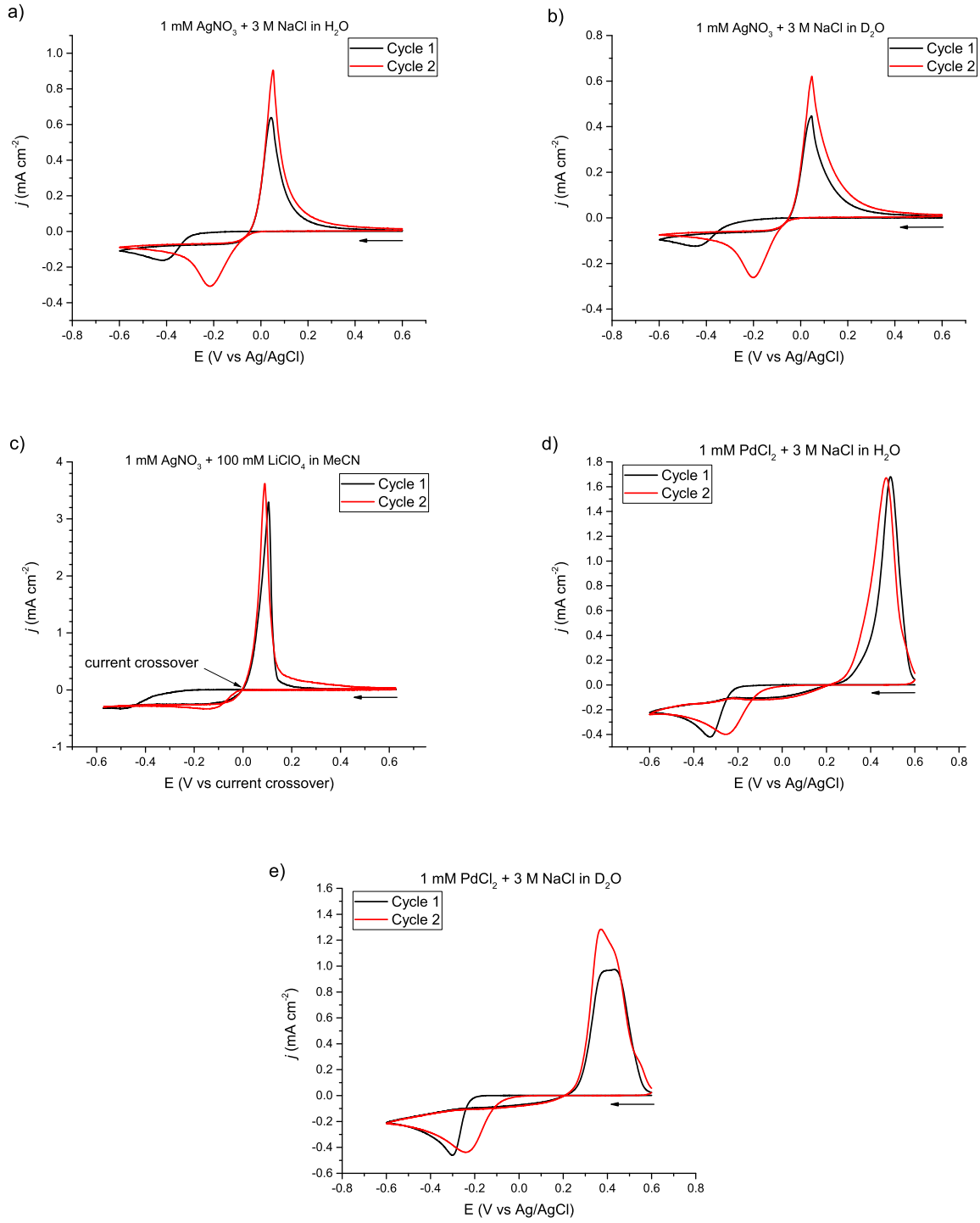

Fig. 1. Cyclic voltammograms for silver (a-c) in H_2O, D_2O and MeCN, respectively, and for palladium (d-e) in H_2O and D_2O, respectively, with pencil graphite electrode acquired at 50 mV/s. All voltammograms show the electrodeposition starting at lower overpotential due to leftover metal deposits on the electrode surface on the second scan.

the metal species. Typically, metal deposition on same metal has lower activation energy than deposition on carbon, so required overpotential for nucleation is lower on the second scan. This has been observed before for Ag [46,47] and Pd [48,49], and also for Au [50] and Cu [51].

3.2. Nucleation

The early stages of Ag and Pd electrodeposition on pencil graphite were examined with chronoamperometry by taking deposition potential steps E_d, from 0,6 V→ E_d→ 0,6 V vs Ag/AgCl RE, where the initial and final potentials were applied for 30 seconds respectively and E_d was applied for 10 seconds as at $t > 10$ s the convective effects take the reaction off from purely diffusion controlled regime [52]. The E_d potentials were chosen around the voltammetric peaks observed in the cyclic voltammogram of each sample. At $t < 1$ s, the charging of the double layer has the dominating contribution to the current density, resulting in a high initial current that rapidly decays. At the same time, the current starts rising due to the formation of active nucleation sites, and the growth of the metal deposits reach its maximum I_{max} at t_{max}, when the diffusion zones around individual nuclei have merged with the neigh-

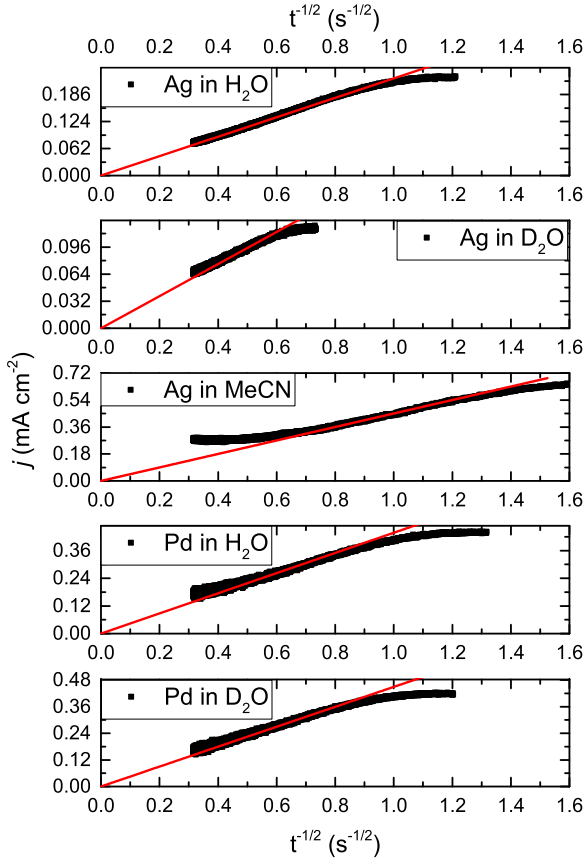

Fig. 2. Current transients of the liquid samples from Table 1 recorded at -410 mV, -410 mV, -510 mV, -300 mV and -300 mV vs Ag/AgCl in descending order as a function $t^{-1/2}$ show linear relationships, indicating that the system is in diffusion control.

boring ones [49,53]. After t_{max} the current decays in linear manner with respect to $t^{-1/2}$, indicating the system to be mostly in diffusion control, as seen in Fig. 2 [48,54], with Ag in MeCN showing a deviation from linearity at longer time periods which could be attributed to earlier onset of natural convection arising from much greater partial molar volume of Ag in MeCN (-20 $cm^3\ mol^{-1}$ [55]) when compared to Ag in aqueous solution (-6,2 $cm^3\ mol^{-1}$ [56]) [57].

3.2.1. Current-time transients

According to the model formulated by Scharifker and Hills (SH-model) [12], there are two different nucleation mechanisms that can be used to describe the formation and growth of the nuclei. If all the nuclei are present from the beginning and grow at the same rate, the process is called *instantaneous nucleation*. On the other hand, if new nuclei are formed during the electrodeposition process, leading to different sizes and growth rates, the process is known as *progressive nucleation*. They proposed that the nucleation mechanism can be observed by rendering the curves dimensionless, achieved by scaling the peak current I_{max} and peak time t_{max} to acquire Eq. (2) and Eq. (3)

$$\frac{I^2}{I_{max}^2} = \frac{1,9542}{t/t_{max}}\left\{1-\exp\left[-1,2564(t/t_{max})\right]\right\}^2 \text{ for instantaneous nucleation, and} \quad (2)$$

$$\frac{I^2}{I_{max}^2} = \frac{1,2254}{t/t_{max}}\left\{1-\exp\left[-2,3367(t/t_{max})^2\right]\right\}^2 \text{ for progressive nucleation.} \quad (3)$$

Scaling the chronoamperometric data by I_{max} and t_{max} the dominating nucleation mechanism can be seen by comparing the data to these theoretical curves. In Fig. 3 the dimensionless plots are represented for Ag in H_2O, D_2O and MeCN and for Pd in H_2O and D_2O, and it can be seen that both Ag and Pd follow the progressive nucleation mechanism in all solvents matching the literary sources for Pd [48,52,58] and for Ag [59,60] in H_2O and D_2O. Although Mele et al. [61] have reported in a similar system the process being instantaneous in 100% MeCN solution with becoming more progressive at higher overpotentials matching the potentials used in our measurements or when increasing H_2O concentration of the solvent. The deviation of Pd curve from Eq. (3) at longer times could be due to concurrent catalysis of proton reduction which can reduce the current by creating a saturated H_{upd} layer of adsorbed H/D inhibiting additional metal deposition [62].

Furthermore, the kinetic parameters in nucleation and growth process can be acquired by utilizing the model developed by Heerman and Tarallo [21] by which values for nucleation constant per site A, number density of active sites on the electrode surface N_0, and the diffusion coefficient D, can be obtained by fitting the experimental data to the following expression for current density:

$$j(t) = zFDc\frac{1}{(\pi Dt)^{1/2}}\frac{\Phi}{\Theta}\left(1-\exp\left[-\alpha N_0(\pi Dt)^{1/2}t^{1/2}\Theta\right]\right), \quad (4)$$

where

$$\Phi = 1-\frac{\exp(-At)}{(At)^{1/2}}\int_0^{(At)^{1/2}}\exp\left(\lambda^2\right)d\lambda \quad (5)$$

$$\Theta = 1-\frac{\left(1-e^{-At}\right)}{At}, \quad (6)$$

with $\alpha = 2\pi(2MDc/\rho)^{1/2}$, c: bulk concentration of the metal precursor, and M and ρ being the molar mass and density of the deposited metal, respectively. The model gives reasonably accurate fits in the potential range of the measurements, as can be seen in Fig. 4 for Pd electrodeposition in D_2O. For other samples the images are located in Figures S1-4 in the supplementary info. The acquired kinetic parameters are plotted as a function of the overpotential in Fig. 5. The corresponding numerical values can be found in tables S1-5 in the supplementary info. From the results it can be concluded that N_0 increases when more negative overpotentials were applied and that there exists an energy distribution of site activation, where larger fraction of sites are activated when increasing the cathodic overpotential [63]. In Fig. 5a for silver electrodeposition, it is noted that the nucleation rate constant per site A follows the trend of being linear as a function of overpotential on logarithmic scale as reported by Alvarez and Salinas [48], and Sebastián et al. [59].

For Ag solution in H_2O nucleation rate constant A matches well with the value reported by Miranda-Hernández et al. [64] for highly oriented pyrolitic graphite (HOPG) electrode within the potential region of their measurements, while to the best knowledge of the authors these values have not been reported for Ag deposition from D_2O or MeCN, both of which seem to behave similarly with respect to increasing the overpotential. In Pd samples, Fig. 5c, the slope seems to be mostly the same for both isotopes but H_2O shows clearly higher nucleation rates compared to D_2O. For Ag the diffusion coefficients were extracted from Eq. (4) and had the values $1,49 \pm 0,22 \cdot 10^{-5}\ cm^2s^{-1}$, $1,05 \pm 0,20 \cdot 10^{-5}\ cm^2s^{-1}$ and $1,07 \pm 0,41 \cdot 10^{-4}\ cm^2s^{-1}$ in H_2O, D_2O and MeCN, respectively. It can be seen that movement in D_2O is relatively sluggish with respect to H_2O, possibly contributing to the observed kinetic effects. For Pd the difference was lower as the diffusion coefficients were $1,62 \pm 0,16 \cdot 10^{-5}\ cm^2s^{-1}$ and $1,71 \pm 0,16 \cdot 10^{-5}\ cm^2s^{-1}$ in H_2O and D_2O, respectively. Plots for the diffusion coefficients as functions of overpotential can be found in Figures S5 and S6 of the supplementary info. Values for A and N_0 for Pd deposition from D_2O have not been reported, but Espino-López et al. [58] reported similar values for A and even greater values for N_0 when making Pd nanoparticles from deep eutectic solutions. Number densities of active sites for Ag Fig. 5b and Pd, Fig. 5d are clearly increasing non-linearly with respect to increasing overpotential. This is

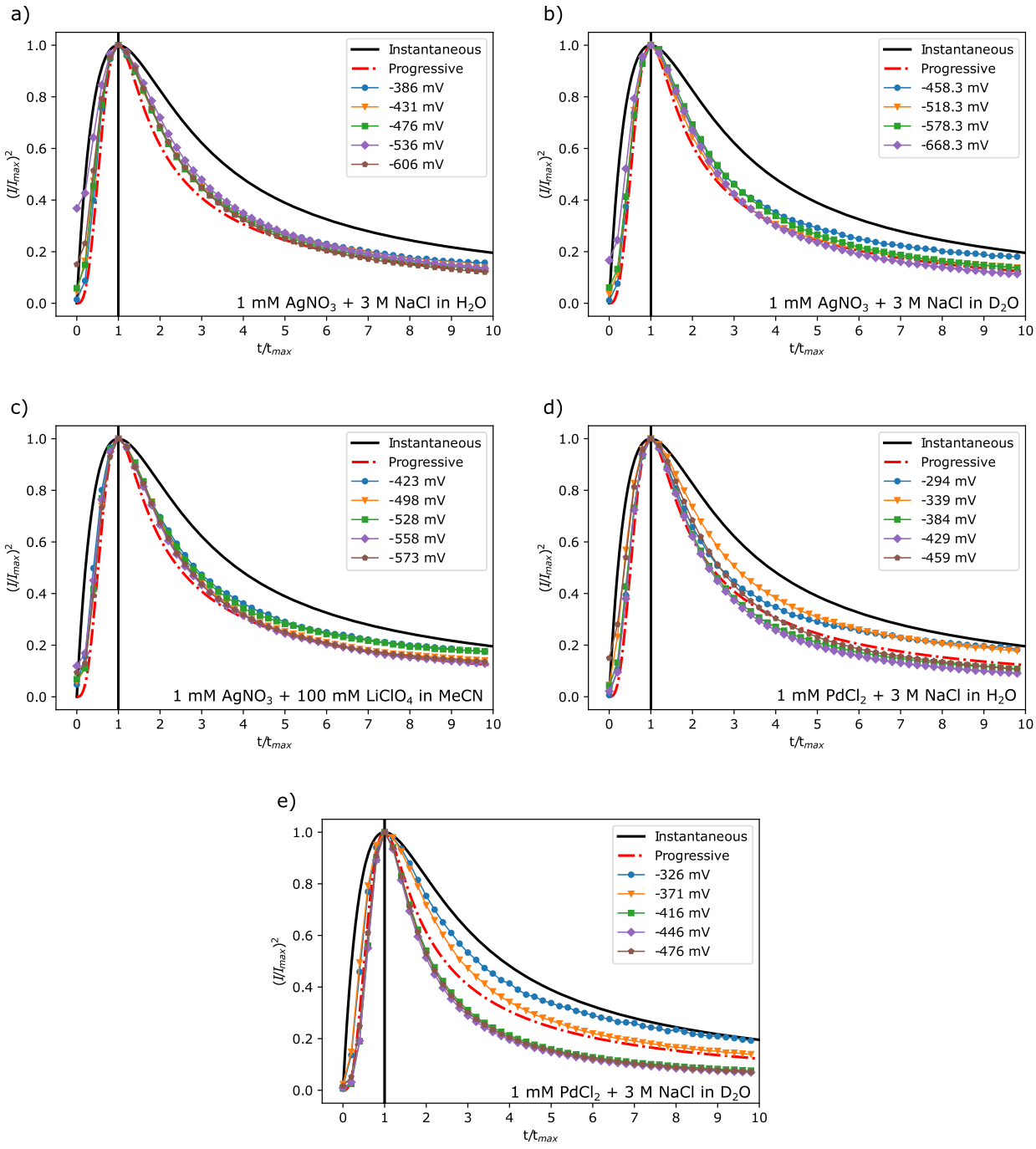

Fig. 3. Normalized current transient of chronoamperometric measurements at different overpotentials for silver (a-c) in H_2O, D_2O, and MeCN, respectively, and for palladium (d-e) in H_2O and D_2O, respectively, compared to the theoretical dimensionless plots for instantaneous (black solid line) and progressive (red dash-dotted line) nucleation from Eqs. (2) and (3). It can be seen that the electrodeposition process for Ag in all solvents and potentials fits the SH-model well and that the progressive nucleation mechanism is dominating. Pd also mostly follows progressive mechanism but especially D_2O based solutions show deviations from the theoretical guidelines.

widely reported in literature [17,48,65,66] and it has been suggested that activation of nucleation sites follows a non-linear distribution as function of overpotential dependent of electrode surface conditions on glassy carbon [67]. Our results would indicate that also the solvent and its isotope has an effect on the underlying activation distribution.

It is clear from the experiments that the slope of nucleation rate constant per site A vs. overpotential is higher in H_2O than in D_2O or MeCN for Ag or in D_2O for Pd. In the aqueous solutions both Ag^+ and Pd^{2+} are complexed with chloride, and surrounded by solvation shell, whereas in MeCN Ag^+ is complexed with CH_3CN [61,68]. If we consider the thermodynamics of the processes, cations need to shed their solvation shells and the complexes during metal deposition to form nuclei. Enthalpy of transfer of Ag^+ and small cations like Na^+ etc. large anions such as I^- or tetraphenylborate from H_2O to D_2O are slightly positive (<3 kJ/mol) while transfer of small anions such as chloride are slightly negative [69], and similarly from H_2O to MeCN [70,71], i.e. it appears that the process should be easier in D_2O and MeCN. However, the entropies of transfer have not been reported, so the Gibbs energy of

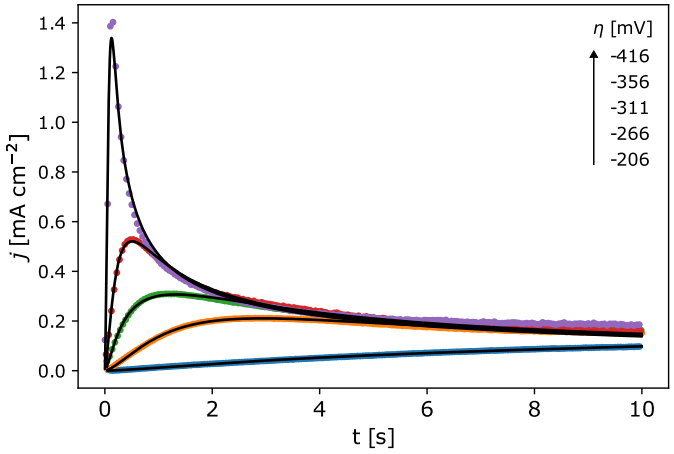

Fig. 4. Experimental potentiostatic current transients (dots) from the electrodeposition of 1 mM $PdCl_2$ with 3 M KCl in D_2O at room temperature at varying overpotentials η, with the theoretical evaluation of Eq. (4) for each transient (lines) used to acquire values for the nucleation rate constant per site A and the number density of active sites N_0.

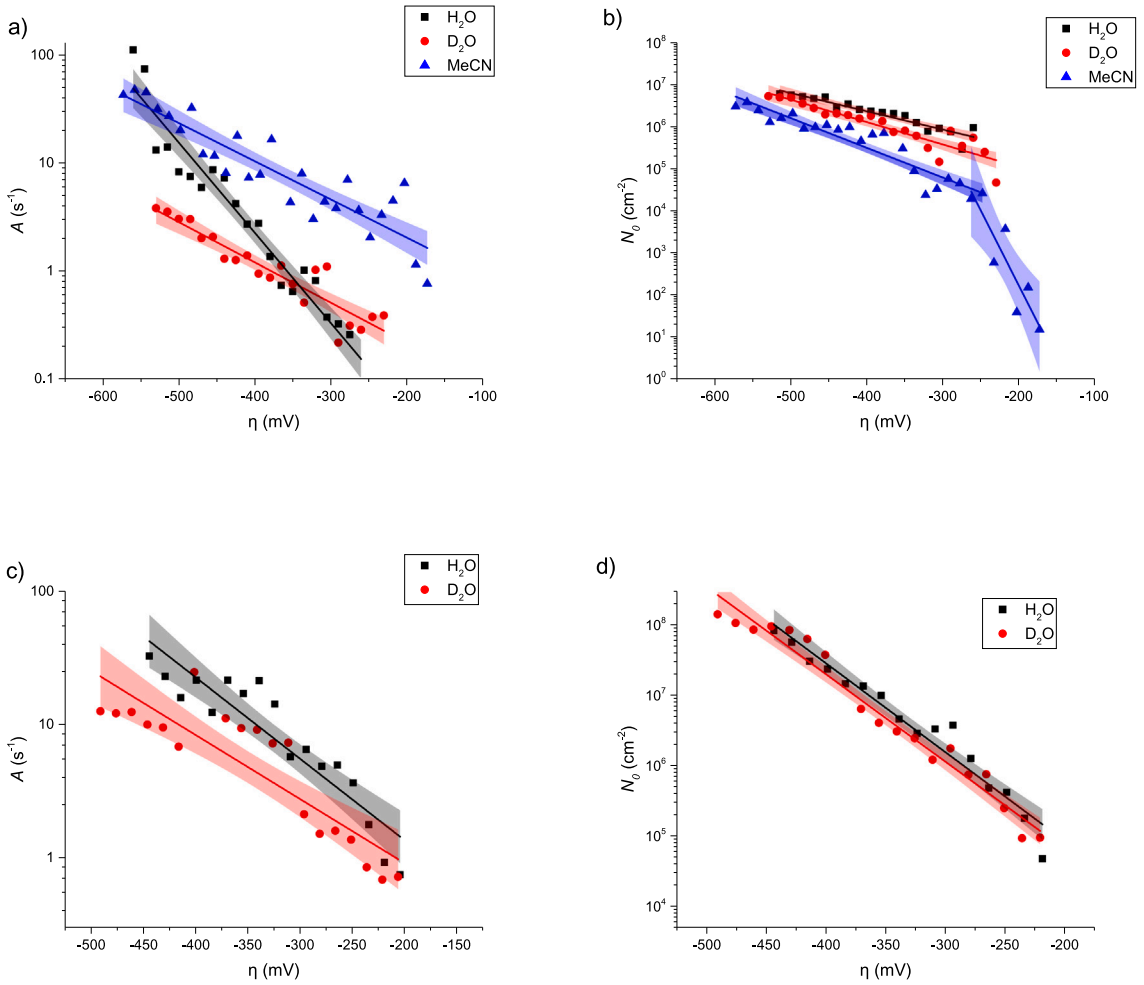

Fig. 5. Values obtained from fitting Eq. (4) to the experimental current transients of graphite electrode on logarithmic scale with 95% confidence bands. a) Nucleation rate constants per site A vs overpotential for 1 mM $AgNO_3$ + 3 M NaCl in H_2O (black), in D_2O (red) and 1 mM $AgNO_3$ + 100 mM $LiClO_4$ in MeCN (blue) and b) the corresponding number densities of nucleation sites N_0. c) Nucleation rate constants per site A vs η for 1 mM $PdCl_2$ + 3 M NaCl in H_2O (black) and in D_2O (red) and d) the corresponding number densities of nucleation sites N_0.

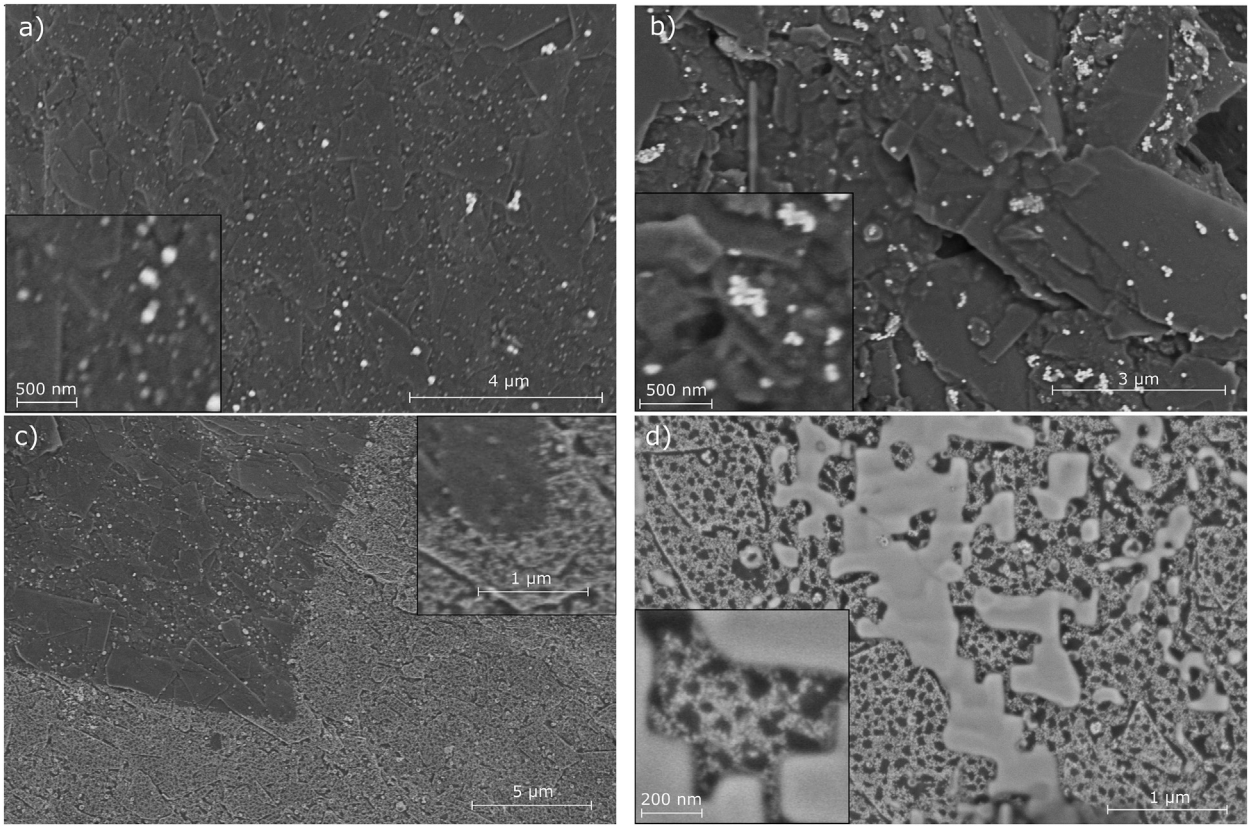

Fig. 6. SEM micrographs obtained with 2 kV accelerating voltage and 25 pA current using T1 backscattering detector for a) Ag deposit from H_2O on pencil graphite surface at -0.470 V vs Ag/AgCl for 10 seconds showing grown Ag islands as bright spots. b) similar although smaller pits are visible for Ag deposit from D_2O at -0.470 V vs Ag/AgCl RE. c) Deposition of Pd from H_2O at -0.270 V vs Ag/AgCl for 10 seconds shows regions separate regions with and without deposition. The areas without deposition were mostly likely under a since detached clay particle. d) Deposition of Pd from D_2O at -0.405 V vs Ag/AgCl for 10 seconds where it can be seen that in certain areas Pd nuclei have grown together and continued plating in uniform layers.

transfer is not known. As the equilibrium potential difference between H_2O and D_2O solutions was negligible, it seems that thermodynamic effects cannot explain the observed differences. D_2O is 20% more viscous than H_2O, so the difference might arise simply from the slower reorganization of the hydration shell and the chloride ions [72]. One kinetic limitation could be how fast the solvent molecules reorganize around the nucleation site and around the released complexing agents, although the difference in solvent reorganization energies between the two isotopes was evaluated as less than 1%, see supplementary info for the calculation.

Nucleation site densities seem to be slightly smaller for Ag in D_2O and much smaller in MeCN, while no significant difference is observed for Pd. The differential capacitance in D_2O is slightly smaller than in H_2O [39], most likely because of the stronger hydrogen bonding network in D_2O, as well as lesser interaction of D_2O with the electrode surface [73]. Based on this, it could be expected that nucleation should be easier in D_2O, resulting in higher density of nucleation sites. It is possible that more chloride is specifically adsorbed on the electrode in D_2O, blocking some of the active nucleation sites. Alternatively, higher viscosity of D_2O could also influence how fast nucleation sites can be freed from chloride, reducing the initial number of sites compared to H_2O. While the nucleation should be easier in MeCN due to its lower double layer capacitance [74] and lower viscosity [75], the reduced nucleation site density in MeCN can be explained by organic solvent molecules being preferentially adsorbed to the metal surface inhibiting reactant adsorption [61]. Unfortunately, we are not aware of any studies on viscosity effects on the nucleation and growth rates during electrodeposition. Clearly, more work is required to fully understand the observed effects.

3.3. Surface morphology of the deposited metals

The surface morphology of the graphite electrodes after deposition was examined with a scanning electron microscope to detect Ag and Pd deposits, as seen in Fig. 6. In Ag deposition, shown in Figs. 6a and 6b, spherical metal deposits with largest diameters around 130 nm are observed to be deposited from H_2O, and average diameter of 80 nm from D_2O with greater aggregation compared to H_2O. Similar larger spherical metallic deposits are not seen for Pd deposition from either isotope solvent, Figs. 6c and 6d, the individual nuclei are of different sizes in the order of 20 nm with some exclusion zones in between that could be attributed to bubble formation due to hydrogen/deuterium evolution. There were difficulties in detecting the surface with the SEM setup used as the supporting carbon ionized by the electron beam starts to agglomerate on top of the deposited Pd when focusing the beam and correcting for astigmatism. It can be seen that in Pd deposited from D_2O, some regions Pd nuclei grow together and start forming a layer. This could explain along with concurrent hydrogen/deuterium evolution, why the normalized current transient at higher overpotentials seen in Fig. 3e do not match that of either supposed nucleation mechanism. The area in Fig. 6c without deposition is taken to have been covered by a clay fragment that has detached between the electrodeposition and taking of the SEM images. Similar fragments have been observed on pencil graphite surface also in some other images.

4. Conclusions

In this work, electrodeposition of Ag and Pd on pencil graphite in H_2O, D_2O and MeCN was examined through cyclic voltammetry and chronoamperometry. Chronoamperometric measurements showed that

the electrodeposition process for all samples was under diffusion control and that the dominating nucleation mechanism was progressive nucleation mechanism as described by Scharifker–Hills-model. By non-linear curve fitting of a theoretical model to the current transients, the kinetic parameters of nucleation rate constant and number density of active sites were obtained and compared to trends observed in literature. Clear differences in the kinetic parameters during deposition from different solvents could be seen, as well as that the isotope of the water has an observable effect on the activation and growth of active sites. SEM images obtained from the pencil graphite surface showed spherical metal deposits of Ag, and much smaller nuclei of Pd, some of which had grown together and started to plate in layers. Kinetic parameters describe the evolution of electrodeposition processes and utilizing different solvent isotope composition could allow to manipulate the evolution of electrodeposition process without changing the chemical properties for manufacturing new materials.

CRediT authorship contribution statement

Kimmo Pyyhtiä: Data curation, Formal analysis, Investigation, Methodology, Software, Validation, Visualization, Writing – original draft, Writing – review & editing. **Pekka Peljo:** Conceptualization, Funding acquisition, Methodology, Project administration, Resources, Supervision, Validation, Writing – review & editing.

Declaration of competing interest

The authors declare that they have no known competing financial interests or personal relationships that could have appeared to influence the work reported in this paper.

Acknowledgements

The authors would like to acknowledge the Materials Research Infrastructure (MARI) at University of Turku for access and support with the SEM and electrochemical facilities. We would also like to thank Vivi Sirén for her exploratory laboratory measurements and Dr. Mattinen for her support during the experiment and writing process. In addition the funding provided from the European Union's Horizon 2020 research and innovation program under grant agreement HERMES No. 952184 is acknowledged.

Appendix A. Supplementary material

Supplementary material related to this article can be found online at https://doi.org/10.1016/j.jelechem.2023.117759.

References

[1] Nor Dyana Zakaria, et al., Effect of supporting background electrolytes on the nanostructure morphologies and electrochemical behaviors of electrodeposited gold nanoparticles on glassy carbon electrode surfaces, ACS Omega (ISSN 2470-1343) 6 (38) (2021) 24419–24431, https://doi.org/10.1021/acsomega.1c02670.

[2] Orest Kuntyi, et al., Pulse electrodeposition of palladium nanoparticles onto silicon in DMSO, J. Chem. (ISSN 2090-9071) 2019 (2019) 4, https://doi.org/10.1155/2019/5859204.

[3] Ishrat Sultana, et al., Electrodeposition of silver (Ag) nanoparticles on MnO2 nanorods for fabrication of highly conductive and flexible paper electrodes for energy storage application, J. Mater. Sci., Mater. Electron. (ISSN 1573-482X) 29 (24) (2018) 20588–20594, https://doi.org/10.1007/s10854-018-0194-7.

[4] Rong Wang, et al., Electrodeposition of Ag nanodendrites SERS substrates for detection of malachite green, Microchem. J. (ISSN 0026-265X) 150 (2019) 104127, https://doi.org/10.1016/j.microc.2019.104127.

[5] Haytham E.M. Hussein, et al., Controlling palladium morphology in electrodeposition from nanoparticles to dendrites: via the use of mixed solvents, Nanoscale (ISSN 2040-3372) 12 (42) (2020) 21757–21769, https://doi.org/10.1039/d0nr05630h.

[6] Emilie Perre, et al., Direct electrodeposition of aluminium nano-rods, Electrochem. Commun. (ISSN 1388-2481) 10 (10) (2008) 1467–1470, https://doi.org/10.1016/j.elecom.2008.07.032.

[7] U.S. Mohanty, Electrodeposition: a versatile and inexpensive tool for the synthesis of nanoparticles, nanorods, nanowires, and nanoclusters of metals, J. Appl. Electrochem. (ISSN 0021-891X) 41 (3) (2011) 257–270, https://doi.org/10.1007/s10800-010-0234-3.

[8] Darko Grujicic, Batric Pesic, Electrodeposition of copper: the nucleation mechanisms, Electrochim. Acta (ISSN 0013-4686) 47 (18) (2002) 2901–2912, https://doi.org/10.1016/S0013-4686(02)00161-5.

[9] S. Tebbakh, et al., Electrochemical nucleation behaviours and properties of electrodeposited Co – Ni alloy thin films 91 (1) (2013) 17–23, https://doi.org/10.1179/0020296712Z.00000000076.

[10] Bülent M. Başol, Application of Electrochemical Deposition Techniques to Thin Film Solar Cell Processing, Thin Film Solar Technology III, ISSN 0277-786X, vol. 8110, 2011, 81100Q.

[11] Michael E. Hyde, Richard G. Compton, A review of the analysis of multiple nucleation with diffusion controlled growth, J. Electroanal. Chem. (ISSN 1572-6657) 549 (2003) 1–12, https://doi.org/10.1016/S0022-0728(03)00250-X.

[12] Benjamin Scharifker, Graham Hills, Theoretical and experimental studies of multiple nucleation, Electrochim. Acta (ISSN 0013-4686) 28 (7) (1983) 879–889, https://doi.org/10.1016/0013-4686(83)85163-9.

[13] Yunkai Sun, Giovanni Zangari, Commentary and notes on the original derivations of the Scharifker-Hills model, J. Electrochem. Soc. (ISSN 0013-4651) (2023), https://doi.org/10.1149/1945-7111/acb618.

[14] D. Siopa, A. Gomes, Nucleation and growth of ZnO nanorod arrays onto flexible substrates, J. Electrochem. Soc. (ISSN 0013-4651) 160 (10) (2013) D476–D484, https://doi.org/10.1149/2.088310jes.

[15] Gerko Oskam, Philippe M. Vereecken, Peter C. Searson, Electrochemical deposition of copper on n-Si/TiN, J. Electrochem. Soc. 146 (4) (1999) 1436, https://doi.org/10.1149/1.1391782.

[16] M. Jayakumar, et al., Electrochemical behavior of ruthenium (III), rhodium (III) and palladium (II) in 1-butyl-3-methylimidazolium chloride ionic liquid, Electrochim. Acta (ISSN 0013-4686) 54 (26) (2009) 6747–6755, https://doi.org/10.1016/j.electacta.2009.06.043.

[17] Aleksandar Radisic, et al., Nucleation and growth of copper on TiN from pyrophosphate solution, J. Electrochem. Soc. (ISSN 0013-4651) 148 (1) (2001) C41, https://doi.org/10.1149/1.1344539.

[18] Mangesh Pise, et al., Instantaneous-progressive nucleation and growth of palladium during electrodeposition, Results Surf. Interf. (ISSN 2666-8459) 6 (2022) 100044, https://doi.org/10.1016/j.rsurfi.2022.100044.

[19] M. Palomar-Pardavé, et al., Nucleation and diffusion-controlled growth of electroactive centers: reduction of protons during cobalt electrodeposition, Electrochim. Acta (ISSN 0013-4686) 50 (24) (Aug. 2005) 4736–4745, https://doi.org/10.1016/j.electacta.2005.03.004.

[20] Gong Luo, et al., Current transition of nucleation and growth under diffusion-controlled electrocrystallization: a brief review, Coatings (ISSN 2079-6412) 12 (8) (2022) 1–14, https://doi.org/10.3390/coatings12081195.

[21] Luc Heerman, Anthony Tarallo, Theory of the chronoamperometric transient for electrochemical nucleation with diffusion-controlled growth, J. Electroanal. Chem. (ISSN 1572-6657) 470 (1) (1999) 70–76, https://doi.org/10.1016/S0022-0728(99)00221-1.

[22] B.R. Scharifker, J. Mostany, Three-dimensional nucleation with diffusion controlled growth Part I. Number density of active sites and nucleation rates per site, J. Electroanal. Chem. 177 (1984) 13–23, https://doi.org/10.1016/0022-0728(84)80207-7.

[23] M. Sluyters-Rehbach, et al., The theory of chronoamperometry for the investigation of electrocrystallization. Mathematical description and analysis in the case of diffusion-controlled growth, J. Electroanal. Chem. (ISSN 0022-0728) 236 (1-2) (1987) 1–20, https://doi.org/10.1016/0022-0728(87)88014-2.

[24] J. Halpern, Mechanisms of electron transfer and related processes in solution, Q. Rev., Chem. Soc. 15 (2) (1961) 207–236, https://doi.org/10.1039/QR9611500207.

[25] N. Sutin, J.K. Rowley, R.W. Dodson, Chloride complexes of iron (iii) ions and the kinetics of the chloride-catalyzed exchange reaction between iron (ii) and iron (iii) in light and heavy water, J. Phys. Chem. 65 (7) (1961) 1248–1252, https://doi.org/10.1021/j100825a037.

[26] Henry Taube, Electron Transfer Reactions of Complex Ions in Solution, Elsevier Inc., 1970, https://doi.org/10.1016/B978-0-12-683850-3.X5001-8.

[27] B.E. Conway, Transactions of the Symposium on Electrode Processes, Wiley, 1961, p. 267.

[28] Mark Salomon, Primary and solvent isotope effects in the anodic evolution of oxygen, J. Electrochem. Soc. 114 (9) (1967) 922, https://doi.org/10.1149/1.2426779.

[29] B.E. Conway, M. Salomon, Studies on the hydrogen evolution reaction down to—150 C and the role of proton tunneling, J. Chem. Phys. 41 (10) (1964) 3169–3177, https://doi.org/10.1063/1.1725692.

[30] M. Salomon, B.E. Conway, Reaction rate and separation factor isotope effects in the hydrogen evolution reaction, Ber. Bunsenges. Phys. Chem. 69 (8) (1965) 669–674, https://doi.org/10.1002/bbpc.19650690804.

[31] Lev I. Krishtalik, Kinetic isotope effect in the hydrogen evolution reaction, Electrochim. Acta (ISSN 0013-4686) 46 (19) (2001) 2949–2960, https://doi.org/10.1016/S0013-4686(01)00526-6.

[32] M.M. Ghoneim, S. Clouser, E. Yeager, Oxygen reduction kinetics in deuterated phosphoric acid, J. Electrochem. Soc. (ISSN 0013-4651) 132 (5) (1985) 1160–1162.

[33] M.M. Jaksic, B. Johansen, R. Tunold, Electrochemical behaviour of platinum in alkaline and acidic solutions of heavy and regular water, Int. J. Hydrog. Energy (ISSN 0360-3199) 18 (10) (1993) 817–837, https://doi.org/10.1016/0360-3199(93)90136-X.
[34] M.M. Jaksic, B. Johansen, R. Tunold, Electrochemical behaviour of iridium in alkaline and acidic solutions of heavy and regular water, Int. J. Hydrog. Energy (ISSN 0360-3199) 19 (4) (1994) 321–335, https://doi.org/10.1016/0360-3199(94)90064-7.
[35] M.M. Jaksic, B. Johansen, R. Tunold, Electrochemical behaviour of palladium in acidic and alkaline solutions of heavy and regular water, Int. J. Hydrog. Energy (ISSN 0360-3199) 18 (2) (1993) 111–124, https://doi.org/10.1016/0360-3199(93)90197-I.
[36] M.M. Jaksic, B. Johansen, R. Tunold, Electrochemical behaviour of rhodium in alkaline and acidic solutions of heavy and regular water, Int. J. Hydrog. Energy (ISSN 0360-3199) 19 (1) (1994) 35–51, https://doi.org/10.1016/0360-3199(94)90176-7.
[37] Edmund C.M. Tse, et al., Observation of an inverse kinetic isotope effect in oxygen evolution electrochemistry, ACS Catal. (ISSN 2155-5435) 6 (9) (2016) 5706–5714, https://doi.org/10.1021/acscatal.6b01170.
[38] Michael J. Weaver, Paul D. Tyma, Scott M. Nettles, Solvent isotope effects upon the kinetics of some simple electrode reactions, J. Electroanal. Chem. Interfacial Electrochem. (ISSN 0022-0728) 114 (1) (1980) 53–72, https://doi.org/10.1016/S0022-0728(80)80435-9.
[39] Roger Parsons, Robert M. Reeves, Paul N. Taylor, The electrical double layer in D2O, J. Electroanal. Chem. Interfacial Electrochem. (ISSN 0022-0728) 50 (1) (1974) 149–152, https://doi.org/10.1016/S0022-0728(74)80287-1.
[40] Jay R. Black, et al., Electrochemical isotope effect and lithium isotope separation, J. Am. Chem. Soc. (ISSN 0002-7863) 131 (29) (2009) 9904–9905, https://doi.org/10.1021/ja903926x.
[41] Satoshi Yanase, Wakana Hayama, Takao Oi, Lithium isotope effect accompanying electrochemical intercalation of lithium into graphite, Z. Naturforsch. A 58 (5-6) (2003) 306–312, https://doi.org/10.1515/zna-2003-5-610.
[42] Makoto Fujie, et al., Isotope effects in electrolytic formation of lithium amalgam, J. Nucl. Sci. Technol. 23 (4) (1986) 330–337, https://doi.org/10.1080/18811248.1986.9734990.
[43] Iulia David, Dana-Elena Popa, Mihaela Buleandra, Pencil graphite electrodes: a versatile tool in electroanalysis, J. Anal. Methods Chem. (2017) 1905968, https://doi.org/10.1155/2017/1905968.
[44] Manuel Palomar-Pardavé, et al., Influence of the coordination sphere on the mechanism of cobalt nucleation onto glassy carbon, J. Electroanal. Chem. (ISSN 1572-6657) 443 (1) (1998) 125–136, https://doi.org/10.1016/S0022-0728(97)00496-8.
[45] Milad Rezaei, Seyed Hadi Tabaian, Davoud Fatmehsari Haghshenas, Electrochemical nucleation of palladium on graphene: a kinetic study with an emphasis on hydrogen co-reduction, Electrochim. Acta (ISSN 0013-4686) 87 (2013) 381–387, https://doi.org/10.1016/j.electacta.2012.09.092.
[46] P. Sebastián, E. Vallés, E. Gómez, First stages of silver electrodeposition in a deep eutectic solvent. Comparative behavior in aqueous medium, Electrochim. Acta (ISSN 0013-4686) 112 (2013) 149–158, https://doi.org/10.1016/J.ELECTACTA.2013.08.144.
[47] Melissa Vega-Cartagena, et al., Potential dependent Ag nanoparticle electrodeposition on Vulcan XC-72R carbon support for alkaline oxygen reduction reaction, J. Electroanal. Chem. (ISSN 1572-6657) 891 (2021) 115242, https://doi.org/10.1016/J.JELECHEM.2021.115242.
[48] A.E. Alvarez, D.R. Salinas, Formation of Cu/Pd bimetallic crystals by electrochemical deposition, Electrochim. Acta (ISSN 0013-4686) 55 (11) (2010) 3714–3720, https://doi.org/10.1016/J.ELECTACTA.2010.01.076.
[49] Tibebu Alemu, Birhanu D. Assresahegn, Tesfaye R. Soreta, Tuning the initial electronucleation mechanism of palladium on glassy carbon electrode, Port. Electrochim. Acta (ISSN 0872-1904) 32 (1) (2014) 21–33, https://doi.org/10.4152/pea.201401021.
[50] Deborah J. Lomax, Ian A. Kinloch, Robert A.W. Dryfe, Au electrodeposition on carbon materials, in: Proceedings of the IEEE Conference on Nanotechnology, 2012, pp. 12–15, issn: 19449399.
[51] Chi Chang Hu, Chi Ming Wu, Effects of deposition modes on the microstructure of copper deposits from an acidic sulfate bath, Surf. Coat. Technol. (ISSN 0257-8972) 176 (1) (2003) 75–83, https://doi.org/10.1016/S0257-8972(03)00004-5.
[52] Y. Gimeno, et al., Electrochemical formation of palladium islands on HOPG: kinetics, morphology, and growth mechanisms, J. Phys. Chem. B (ISSN 1089-5647) 106 (16) (2002) 4232–4244, https://doi.org/10.1021/jp014176e.
[53] A.E. Bolzán, Electrodeposition of copper on glassy carbon electrodes in the presence of picolinic acid, Electrochim. Acta (ISSN 0013-4686) 113 (2013) 706–718, https://doi.org/10.1016/J.ELECTACTA.2013.09.132.
[54] Ana.S. Fuentes, A.F. Filippin, M. del C. Aguirre, Pd nucleation and growth mechanism deposited on different substrates, Proced. Mater. Sci. (ISSN 2211-8128) 8 (2015) 541–550, https://doi.org/10.1016/J.MSPRO.2015.04.107.
[55] Yizhak Marcus, Glenn Hefter, Standard partial molar volumes of electrolytes and ions in nonaqueous solvents, Chem. Rev. (ISSN 0009-2665) 104 (7) (2004) 3405–3452, https://doi.org/10.1021/cr030047d.
[56] Yizhak Marcus, Thermodynamics of solvation of ions. Part 6.—The standard partial molar volumes of aqueous ions at 298.15 K, J. Chem. Soc. Faraday Trans. 89 (4) (1993) 713–718, https://doi.org/10.1039/FT9938900713.
[57] Javor K. Novev, Shaltiel Eloul, Richard G. Compton, Influence of reaction-induced thermal convection on the electrical currents measured in chronoamperometry and cyclic voltammetry, J. Phys. Chem. C (ISSN 1932-7447) 120 (25) (2016) 13549–13562, https://doi.org/10.1021/acs.jpcc.6b03413.
[58] I.E. Espino-López, et al., Palladium nanoparticles electrodeposition onto glassy carbon from a deep eutectic solvent at 298 K and their catalytic performance toward formic acid oxidation, J. Electrochem. Soc. (ISSN 0013-4651) 166 (1) (2019) D3205–D3211, https://doi.org/10.1149/2.0251901jes.
[59] Paula Sebastián, et al., Three-dimensional nucleation with diffusion controlled growth: a comparative study of electrochemical phase formation from aqueous and deep eutectic solvents, J. Electroanal. Chem. (ISSN 1572-6657) 793 (2017) 119–125, https://doi.org/10.1016/j.jelechem.2016.12.014.
[60] Bryan H.R. Suryanto, et al., Tuning the electrodeposition parameters of silver to yield micro/nano structures from room temperature protic ionic liquids, Electrochim. Acta (ISSN 0013-4686) 81 (2012) 98–105, https://doi.org/10.1016/j.electacta.2012.07.066.
[61] Claudio Mele, et al., Silver electrodeposition from water-acetonitrile mixed solvents and mixed electrolytes in the presence of tetrabutylammonium perchlorate. Part I-electrochemical nucleation on glassy carbon electrode, J. Solid State Electrochem. (ISSN 1432-8488) 13 (10) (2009) 1577–1584, https://doi.org/10.1007/s10008-008-0732-y.
[62] Yihua Liu, et al., Self-terminating growth of platinum films by electrochemical deposition, Science (ISSN 0036-8075) 338 (6112) (Dec. 2012) 1327–1330, https://doi.org/10.1126/science.1228925.
[63] Rex Louis Deutscher, Stephen Fletcher, Nucleation on active sites. Part IV. Invention of an electronic method of counting the number of crystals as a function of time, and the discovery of nucleation rate dispersion, J. Electroanal. Chem. (ISSN 0022-0728) 239 (1-2) (1988) 17–54, https://doi.org/10.1016/0022-0728(88)80268-7.
[64] M. Miranda-Hernández, I. González, N. Batina, Silver electrocrystallization onto carbon electrodes with different surface morphology: active sites vs surface features, J. Phys. Chem. B (ISSN 1089-5647) 105 (19) (2001) 4214–4223, https://doi.org/10.1021/jp002057d.
[65] J. Mostany, et al., Electrochemical nucleation and the classical theory: overpotential and temperature dependence of the nucleation rate, Russ. J. Electrochem. (ISSN 1023-1935) 44 (6) (2008) 652–658, https://doi.org/10.1134/S1023193508060049.
[66] H. Cesiulis, M. Ziomek-Moroz, Electrocrystallization and electrodeposition of silver on titanium nitride, J. Appl. Electrochem. (ISSN 0021-891X) 30 (11) (2000) 1261–1268, https://doi.org/10.1023/A:1026553712521.
[67] Daniel Torres, et al., Distribution of copper electrochemical nucleation activities on glassy carbon: a new perspective based on local electrochemistry, J. Electrochem. Soc. (ISSN 0013-4651) 169 (10) (2022) 102513, https://doi.org/10.1149/1945-7111/ac9717.
[68] Colin B. Baddiel, Malcolm J. Tait, George J. Janz, Nonaqueous silver nitrate solutions. Spectral studies in acetonitrile, J. Phys. Chem. (ISSN 0022-3654) 69 (10) (1965) 3634–3638, https://doi.org/10.1021/j100894a068.
[69] C.V. Krishnan, H.L. Friedman, Solvation enthalpies of various ions in water and heavy water, J. Phys. Chem. (ISSN 0022-3654) 74 (11) (1970) 2356–2362, https://doi.org/10.1021/j100705a020.
[70] Ewa Kamieńska-Piotrowicz, Halina Inerowicz, Ionic enthalpies of transfer in acetonitrile–water mixtures, J. Chem. Soc. Faraday Trans. 86 (20) (1990) 3391–3394, https://doi.org/10.1039/FT9908603391.
[71] Franz Hörzenberger, Gerhard Gritzner, Gibbs energies, entropies and enthalpies of transfer for monovalent cations from acetonitrile to several solvents, J. Chem. Soc. Faraday Trans. 89 (19) (1993) 3557–3564, https://doi.org/10.1039/FT9938903557.
[72] Robert C. Hardy, Robert L. Cottington, Viscosity of deuterium oxide and water in the range 5 to 125 C, J. Res. Natl. Bur. Stand. (ISSN 0091-0635) 42 (6) (1949) 573, https://doi.org/10.6028/jres.042.049.
[73] Stanisław Lamperski, A theoretical analysis of the Hg/D2O interface, J. Electroanal. Chem. Interfacial Electrochem. (ISSN 0022-0728) 289 (1) (1990) 285–289, https://doi.org/10.1016/0022-0728(90)87223-7.
[74] Koichi Jeremiah Aoki, Jingyuan Chen, Peng Tang, Double layer impedance in mixtures of acetonitrile and water, Electroanalysis (ISSN 1521-4109) 30 (8) (2018) 1626–1633, https://doi.org/10.1002/elan.201800025.
[75] CRC Handbook of Chemistry and Physics, 88th ed, ISBN 0849304881, 2007.